Northumbria Research Link

Northumbria University
NEWCASTLE

University Library

Article

Abrasive Wear Behavior of Al–4Cu–1.5Mg–WC Composites Synthesized through Powder Metallurgy

Gustavo Rodríguez-Cabriales [1], Carlos G. Garay-Reyes [1,*], Juan C. Guía-Tello [2], Hansel M. Medrano-Prieto [3], Ivanovich Estrada-Guel [1], Lilia J. García-Hernández [1], Marco A. Ruiz-Esparza-Rodríguez [1], José M. Mendoza-Duarte [1], Karen A. García-Aguirre [1], Sergio Gonzáles-Sánchez [4] and Roberto Martínez-Sánchez [1,*]

[1] Laboratorio Nacional de Nanotecnología, Centro de Investigación en Materiales Avanzados (CIMAV), Miguel de Cervantes 120, Chihuahua 31136, Mexico
[2] Departamento Metal-Mecánica, Tecnológico Nacional de México/Instituto Tecnológico de Saltillo, Venustiano Carranza 2400, Saltillo 25280, Mexico
[3] Departamento de Nanotecnología, Universidad Tecnológica de Chihuahua Sur, Km. 3.5 Carr. Chihuahua-Aldama, Chihuahua 31313, Mexico
[4] Faculty of Engineering and Environment, Northumbria University, Newcastle upon Tyne NE1 8ST, UK
* Correspondence: carlos.garay@cimav.edu.mx (C.G.G.-R.); rmtzschz@gmail.com (R.M.-S.)

Abstract: Different Al–4Cu–1.5Mg/WC composites were synthesized through powder metallurgy to establish the effect of WC particle addition on the abrasive wear behavior of an Al–4Cu–1.5Mg (wt. %) alloy. The wear tests were performed using a pin-on-disc tribometer at room temperature in dry conditions using SiC abrasive sandpaper as a counterbody and tribometer of linear configuration. The results showed that WC additions increase the hardness of the Al–4Cu–1.5Mg alloy due to the strengthening effect of particle dispersion in the aluminum matrix, which generates an improvement in the wear resistance of the composites by preventing direct contact of the sample with the counterbody, in turn delaying the plastic deformation phenomena responsible for the degradation sequence. In addition, the dominant wear mechanism was abrasive wear, and the increased friction coefficient did not bring a rapid wear rate, which was related to the enhanced deformation resistance due to the high hardness.

Keywords: Al–Cu–Mg alloy; WC; aluminum matrix composites; powder metallurgy; abrasive wear

1. Introduction

Aluminum alloys are widely used to make aerospace and automotive components because of their high specific strength and good formability. Moreover, they are attractive materials for tribological applications due to their low density and high hardening capacity [1–3]. Nevertheless, their use has been limited because of their low mechanical and tribological properties compared with ferrous alloys [4]. For this reason, there is interest in adding different reinforcements to aluminum and its alloys, such as carbides or oxides, to develop aluminum matrix composites (AMCs) that provide additional strength to the parent material and enhance its tribological properties without compromising the specific strength to be able to use these composites for structural applications [5–9]. In this sense, the Al–Cu–Mg system forms an essential part of the 2xxx series alloys. These alloys can play the role of a matrix in composite materials, i.e., aluminum alloys strengthened by the homogeneous dispersion of reinforcing particles, since these alloys show strong interfacial bonds with reinforced particles, thus resulting in an efficient load transfer. This advantage will improve the stiffness, hardness, fatigue resistance, and tribological properties, thus resulting in composites of great interest to manufacturing industrial components such as aircraft fitting, couplings, shafts, and gear materials for industrial applications [5].

The mechanical performance of AMCs depends on the nature of the reinforcing phase, volume fraction, homogeneity of dispersion, and the processing technique employed. Different microstructures and mechanical performances can be achieved depending on the fabrication parameters. AMCs can be fabricated using different processing techniques, including powder metallurgy, spray atomization and co-deposition, plasma spraying, stir casting (composting), and squeeze casting. Among them, stir casting is the most economical process [10]; however, it has certain limitations due to the difference between the densities of the matrix and reinforcing phase(s). These differences can lead to segregation and agglomeration of the reinforcement particles, favoring the formation of stress concentration sites and promoting the generation of cracks, highly localized residual porosity, and weak interfacial bonding [11]. Thus, achieving a homogeneous dispersion of hard particles within the Al matrix is essential, which can be achieved using powder metallurgy (PM). This process enables the improvement of the reaction between the matrix and the reinforcing particles to generate structural and microstructural features typical of the process, such as high dislocation density, small grain size, and high chemical homogeneity, that can prevent or minimize problems associated with agglomeration and improve the alloy's performance [10,12,13].

AMCs are attractive for multiple applications due to their improved properties, such as high specific strength, specific modulus, damping capacity, and good wear resistance, compared to unreinforced alloys. In addition, various investigations reported that ceramic reinforcements, such as SiC and TiC, ZrO, B_4C, and SnO_2, could enhance the tribological properties of aluminum; therefore, they are excellent reinforcements to enhance the wear resistance of AMCs under dry and lubricated conditions [14,15]. WC particles are an excellent reinforcement option among ceramic reinforcements due to their good mechanical properties, wear resistance, and strong interface bonding between WCs and the Al–Cu–Mg matrix [11]. However, although AMCs are excellent candidates for tribological applications, only a few studies have been reported on the Al–Cu–Mg system reinforced with WC particles. For example, Pal et al. [16] studied the effect of WC as a reinforcement but in the form of nanoparticles in the Al matrix. They used ultrasonic cavitation-assisted stir-casting as the preparation method. The Al–Cu–Mg alloy system has more density than pure Al. Therefore, the homogeneous dispersion of reinforcing particles is more difficult to achieve when using the traditional casting method [11,17]. Thus, this research aims to investigate the effects of tungsten carbide (WC) particles on the tribological behavior of an Al–4Cu–1.5Mg (wt. %) alloy matrix using a powder metallurgy route. Moreover, this research is focused on abrasive wear; for this reason, the composites were tested against an abrasive surface (SiC grinding paper). Abrasive wear, i.e., three-body abrasion for which wear is caused by hard debris, has scarcely been explored before [18] and has never been explored for Al–4Cu–1.5Mg–WC composites despite these conditions being frequent in many industrial applications for which the employment of light and wear-resistant materials is of great interest.

2. Materials and Methods

Elemental powder of Al, Cu, Mg, and WC (Table 1) was mixed to obtain the Al–4Cu–1.5Mg (wt. %) alloy and the composites with 1, 2, and 3 WC (wt.%) equivalent to 0.18, 0.36, and 0.54 in volume fraction (%), respectively, using a high-energy ball mill (E-Max).

Table 1. Specifications of the elemental powder used.

Element Powder	Purity (%)	Particle Size (µm)
Al	99.5	<32
Cu	99.5	<32
Mg	99.8	<32
WC	99.9	<1

The conditions for mechanical milling were an argon atmosphere, hardened steel balls with a ball-to-powder ratio of 4 to 1, and 3 mL of methanol as a process control agent. The green compacted samples were obtained with uniaxial pressing into a die with an internal diameter of 40 mm. These samples were, subsequently, sintered in an argon atmosphere at a temperature of 500 °C for 3 h; then, the sintered samples were hot extruded at 490 °C with an extrusion ratio of ~16 to obtain cylindrical bars with a diameter of 9.5 mm and 450 mm length. Finally, samples underwent an annealing process at 420 °C for 3 h; this last step aimed to eliminate the possible residual stresses caused by the previous hot extrusion process and evaluate only the effect of the addition of the WC particles [8]. For comparison purposes, the unreinforced alloy was taken as a reference.

The experimental density of the samples was calculated using Archimedes' principle. The samples were weighed in air and immersed in distilled water using an electronic balance with a precision of ±0.1 mg. The theoretical density was calculated based on the rule of mixtures and is defined in Equation (1).

$$\frac{1}{\rho_{theoretical}} = \sum_{i=1}^{n} \frac{x_i}{\rho_i} \tag{1}$$

where x_i and ρ_i are the weight fraction and density of the ith element, respectively. The ratio of measured density to theoretical density is called relative density and is defined in Equation (2) [19,20].

$$\rho_{Rel} = \frac{\rho_{exp}}{\rho_{th}} \tag{2}$$

where ρ_{exp} and ρ_{th} are the experimental density and theoretical density, respectively. The porosity is the percentage of voids in a sample which can be calculated based on relative density and is defined in Equation (3) [19,20].

$$\% \ porosity = \left(1 - \frac{\rho_{exp}}{\rho_{th}}\right) \times 100 \tag{3}$$

A Panalytical (Malvern, UK) X'Pert PRO brand X-ray diffractometer (40 kV, 35 mA) was used for structural characterization. Vickers microhardness (HV) measurements were performed in a LECO (St. Joseph, MI, USA) LM300AT tester with a load of 100 g and 10 s of dwell time; at least ten indentations were made on each sample, and the reported values are the average values obtained.

Wear tests were performed using two different methods, a commercial tribometer to obtain the friction coefficient and a conventional pin-on-disc method to evaluate the wear rate. A Bruker (Billerica, MA, USA) UMT-3 tribometer was employed for the first method using a linear configuration test (Figure 1a). Samples with 25 × 10 × 4 mm were cut from the extruded bar and polished to a mirror finish. The forces applied to the samples were 3.0 and 5.0 N, with a sliding distance of 5 mm, 10 s per cycle, and using a 100Cr6 hardened chrome steel sphere of 6 mm diameter.

For the pin-on-disc tests (Figure 1b), 10 mm diameter and 20 mm high samples were cut from an extruded bar and prepared using conventional metallography techniques. The samples were placed in a vertical specimen holder against a horizontal rotating disc covered with abrasive mediums with a cantilever system [15,21]. The force applied to the samples was 3.0 and 5.0 N against a steel counterbody (made of hardened tools steel-D2), on which SiC paper was attached to perform the wear tests.
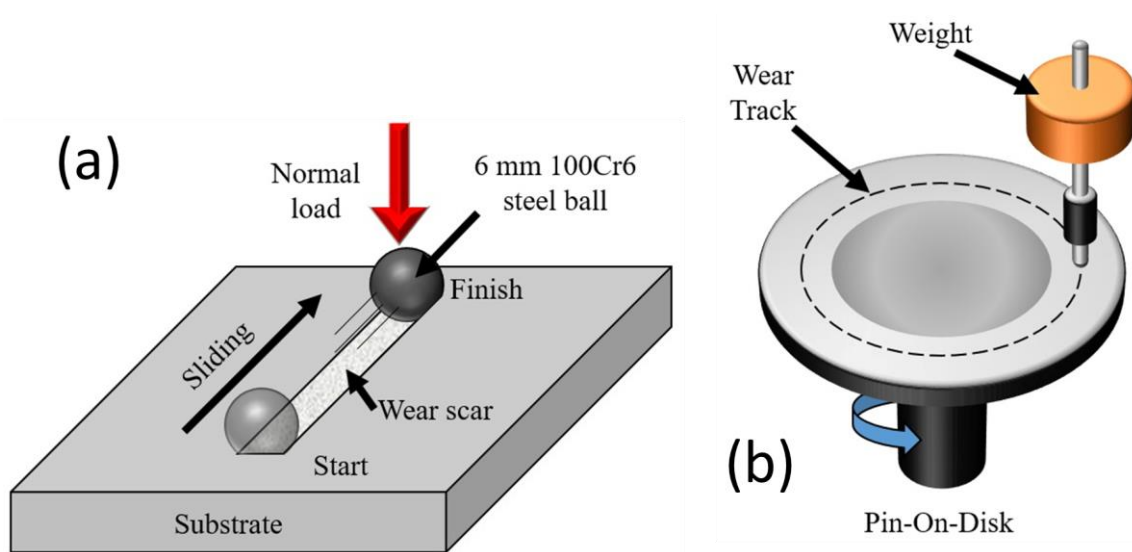
Figure 1. The principle of linear configuration test (**a**) and pin-on-disc tests (**b**).

Different SiC abrasive grit sandpapers were used as abrasive mediums, identified with the numbers 180, 240, and 400 (78, 52, and 22 μm particle size, respectively) according to the modified pin abrasion tester configuration (ASTM G132 standard). The speed of the disc was 2 m/s, the turning radius was 85 mm, and in the contact area of the sample and the SiC abrasive paper, a constant direct flow of water was used as a lubricant to decrease the test temperature and remove the wear debris. The total sliding distance of the pin-on-disc test was 300 m, and after every 100 m, the sample was weighed to obtain the volume loss according to the ASTM G99-17 standard [22]. At least three runs were performed for each test condition, and the average value was reported. The volume loss of the tested samples was calculated using Equation (4), and the worn surface of the tested samples was evaluated using scanning electron microscopy with a Hitachi (Tokyo, Japan) SU 3500 microscope operated at 5 kV. The wear rate values of the samples were calculated according to Equation (5).

$$\text{Volume loss } \left(\text{mm}^3\right) = \frac{\text{Weight loss (g)}}{\text{Density } \left(\text{g/mm}^3\right)} \tag{4}$$

$$\text{Wear rate } \left(\text{mm}^3/\text{N·m}\right) = \frac{\text{Volume loss } \left(\text{mm}^3\right)}{\text{Sliding distance (m) load (N)}} \tag{5}$$

3. Results

3.1. Characterization of the Initial Materials

Figure 2 shows BSE–SEM micrographs corresponding to the initial powders and green and annealing conditions for the Al–4Cu–1.5Mg alloy with 1 wt. % WC. Al-Rich, Cu-Rich, and WC phases were observed for the green condition. However, Al–Cu–Mg, Al_2Cu, and WC phases were observed for the annealing condition. In this sense, the microstructural characterization of the milling and sintering conditions was reported by Rogriguez-Cabriales et al. [11].
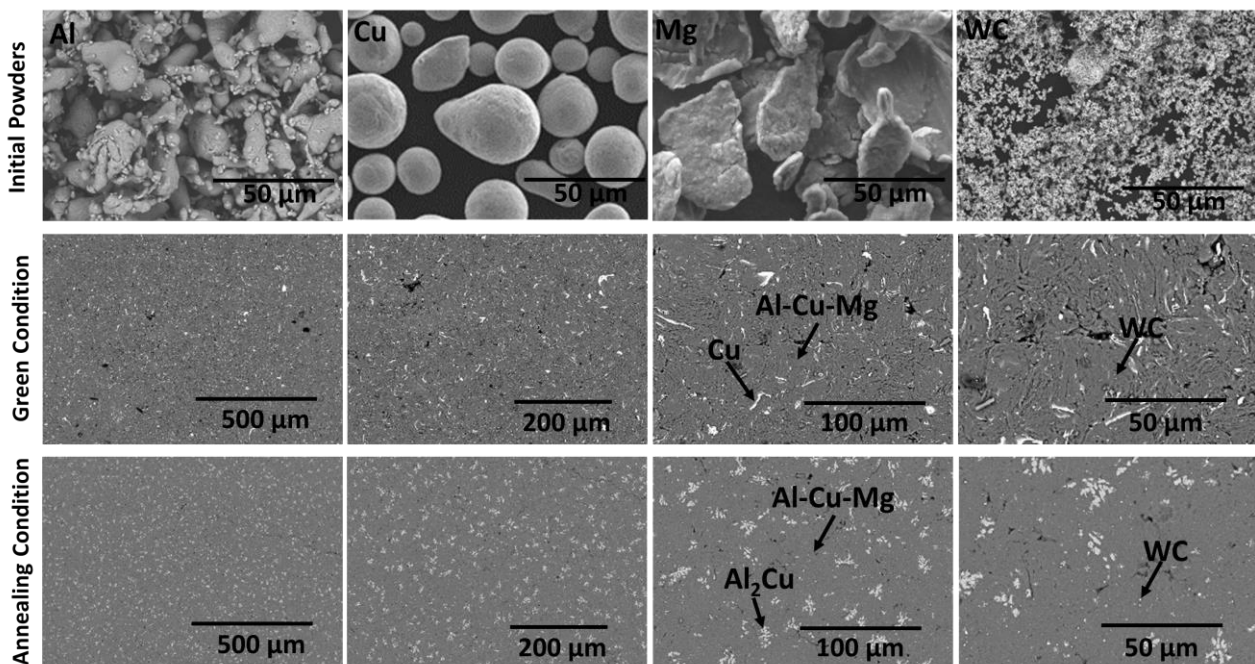
Figure 2. SEM backscattered electron images corresponding to the initial powders and green and annealing conditions for Al–4Cu–1.5Mg alloy with 1 wt. % WC.

Table 2 shows the experimental (i.e., Archimedes density) and theoretical values of density and relative density and porosity (%) of the Al–Cu–Mg alloy and those of the corresponding composites. An increment of the theoretical as a function of WC content was consistent with the higher density of WC (15.63 g/cm^3) than the Al-based matrix's density (2.782 g/cm^3). However, a decrease in Archimedes and relative density was observed, which was attributed to the addition of hard reinforcing particles affecting the compressibility and sinterability of the compacts [23]. The presence of minimum porosities was expected from the calculation of relative density values, which was confirmed by the experimental results (Figure 2 and [11]).

Table 2. Experimental and theoretical density values, relative density, and porosity (%) of the Al–Cu–Mg alloy and the composites with 1, 2, and 3 WC (wt. %).

Sample Name (wt. %)	Theoretical Density (g/cm^3)	Archimedes Density (g/cm^3)	Relative Density	Porosity (%)
Al–4.5Cu–1.5Mg	2.764	2.736 ± 0.010	0.99	1
Al–4.5Cu–1.5Mg + 1%WC	2.787	2.703 ± 0.013	0.97	3
Al–4.5Cu–1.5Mg + 2%WC	2.811	2.642 ± 0.008	0.94	6
Al–4.5Cu–1.5Mg + 3%WC	2.836	2.581 ± 0.0115	0.91	9

Figure 3 shows the XRD patterns of (a) the Al–4.5Cu–1.5Mg + 3WC composite after extrusion and annealing, and (b) the Al–4Cu–1.5Mg alloy with 0, 1, 2, and 3 wt. % WC particles after annealing. Different characteristic peaks of Al, Al$_2$Cu and WC phases were observed in the XRD patterns. Figure 1a shows that the annealing process did not affect the formation of new phases since both XRD patterns were similar. Figure 1b shows peaks corresponding to Al and Al$_2$Cu phases in all samples; the composites show additional peaks corresponding to the WC phase, which increase in intensity as a function of the WC content.
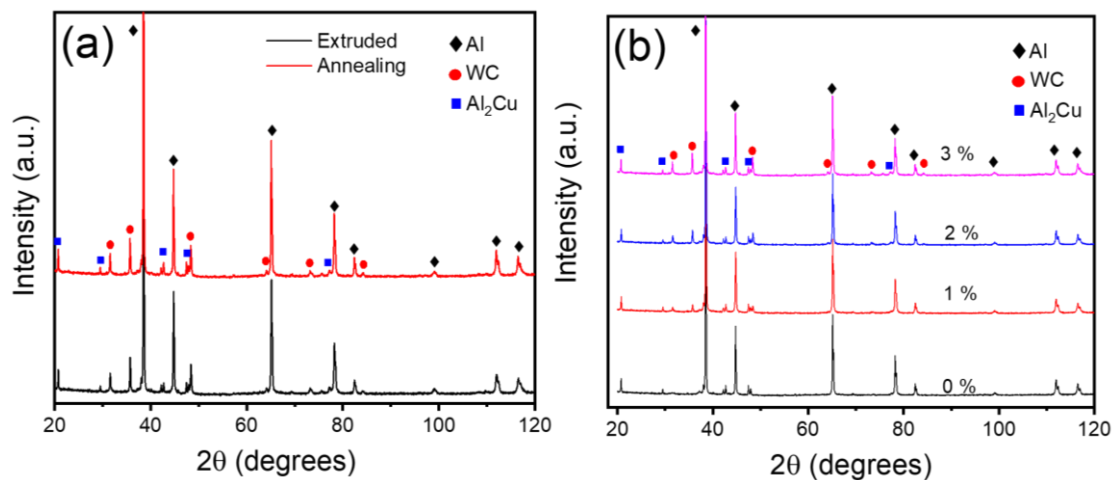
Figure 3. XRD patterns of (**a**) Al–4.5Cu–1.5Mg + 3WC after extrusion and annealing, and (**b**) the Al–4Cu–1.5Mg alloy with 0, 1, 2, and 3 wt. % tungsten carbide (WC) particles after annealing.

3.2. Mechanical and Wear Behavior

3.2.1. Vickers Hardness

The mechanical behavior was assessed using hardness and wear tests. Figure 4 shows the evolution of the Vickers hardness for the parent Al–4Cu–1.5Mg alloy and the corresponding composites with different concentrations of WC (1, 2, and 3 wt. %). All the composites exhibited increased HV with increasing WC content, and their hardness was higher than the Al–4Cu–1.5Mg alloy. A maximum hardness increment of 24 HV from 126 to 150 HV for the sample with the highest WC concentration (3 wt. %) was observed, an enhancement of about 19%.
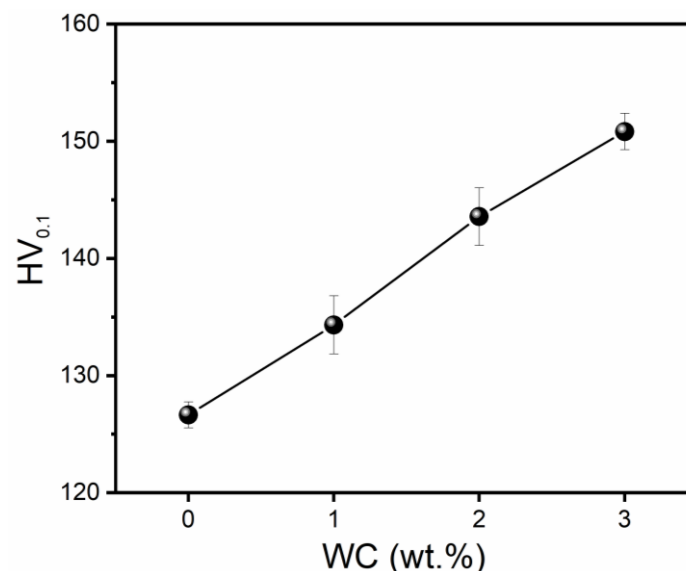
Figure 4. Evolution of the Vickers hardness with WC concentration up to 3 wt. %.

3.2.2. Wear Rate (Pin-On-Disc Tests)

Figure 5 shows the wear rate of the Al–4Cu–1.5Mg alloy and the corresponding composites during the pin-on-disc test at 3 and 5 N. The wear rate values decreased as the number of SiC abrasive sandpaper increased, and the trend was more pronounced at 5 than 3 N load. Moreover, at a larger abrasive grit size (78 µm/180 number sandpaper), a higher value in the wear rate for a load of 5 N and a lower value at higher WC contents in both loads was observed. However, the wear rate value difference tended to be very close

at a smaller abrasive grit size (22 μm/ 180 number sandpaper) in the Al–4Cu–1.5Mg alloy and the composites.
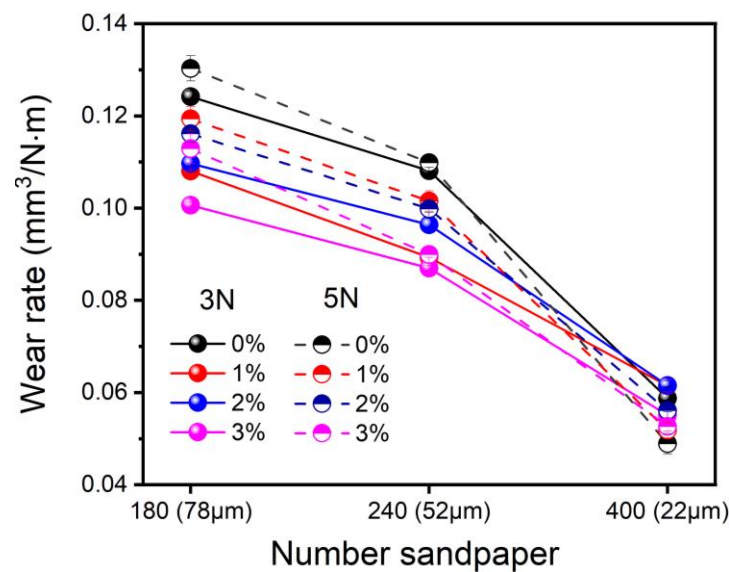

Figure 5. Wear rate of the Al-4Cu-1.5Mg alloy and the composites with 0, 1, 2, and 3 wt. % tungsten carbide (WC) particles for the different sandpaper numbers during the pin-on-disc test at 3 and 5 N.

3.2.3. Coefficient of Friction (Linear Configuration Test)

Figure 6 shows the coefficient of friction (COF) of the Al–4Cu–1.5Mg alloy and the composite Al–4.5Cu–1.5Mg + 3WC after the wear test. Figure 6a shows the evolution of the COF during the sliding time for Al–4.5Cu–1.5Mg alloy and the composite Al–4.5Cu–1.5Mg + 3WC when subjected to a 5 N load. The COF is a valuable parameter for understanding the wear behavior because a small value indicates high wear resistance [24,25]. As generally observed, the COF showed two stages (Figure 6a), an initial rapid increase with time (i.e., unstable stage) followed by a steady-state stage [24]. The first stage exhibited an increment related to static friction since a greater force is required to initiate the sliding movement from rest for the sample and the counterbody in contact. A progressive decrease followed this stage as the sliding distance increased since the sample's surface smoothened over time until the steady condition was reached for the rest of the sliding distance. Figure 6b indicates an increment of the average COF as a function of WC content and higher values for a load of 3 N; this was principally attributed to the hardness, which had a direct relationship with COF [26–28]. Thus, a higher particle volume fraction of WC leads to higher hardness (Figure 4), resulting in a larger COF; it is important to comment that the presence of WC reinforcing particles increase the COF by directly interacting with sandpaper on the counterbody. This behavior was consistent with the friction behavior of most metal-based composite materials [29]. However, it has also been reported that increasing the presence of WC reinforcing particles in coatings that implicated certain grades of fusion resulted in a more refined microstructure [30,31]. This behavior was attributed to the undissolved WC acting as a small heat sink, increasing the nucleation rate, promoting grain nucleation, and increasing the mechanical properties (Vickers hardness) and COF. Nevertheless, since the present work was carried out in a solid state (powder metallurgy), such an effect of grain size on wear behavior can be discarded.
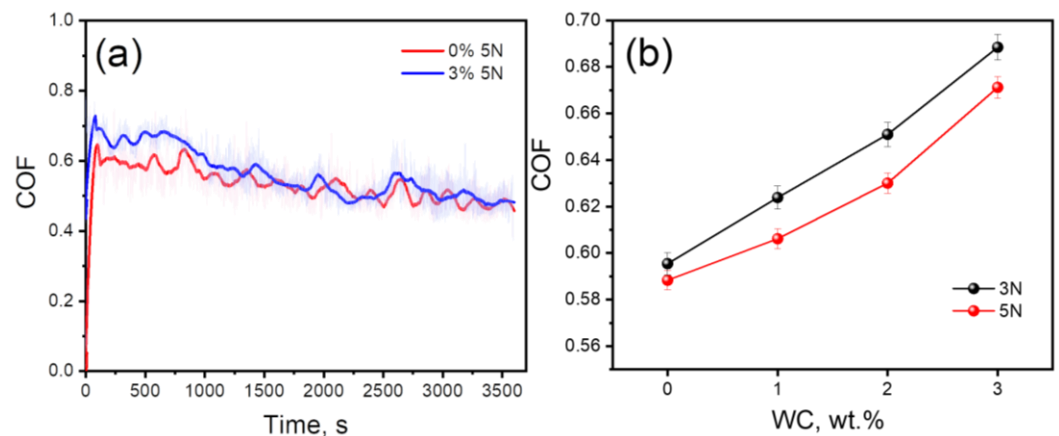
Figure 6. Coefficient of friction (COF) of Al–4Cu–1.5Mg and Al–4Cu–1.5Mg + 3WC composite subjected to 5 N of load (**a**) and the average coefficient of friction (COF) of the composites with 1, 2, and 3 WC (wt. %) after the test at loads of 3 and 5 N (**b**).

3.2.4. Worn Surfaces (Pin-On-Disc Tests)

Figure 7 shows representative SEM secondary electron images from the worn surfaces of the Al–4.5Cu–1.5Mg alloy and the Al–4.5Cu–1.5Mg + 3WC composite. The surfaces of both systems presented patterns of similar grooves along the sliding direction and signs of delamination. However, the Al–4.5Cu–1.5Mg alloy exhibited more significant delamination and wider/deeper grooves with a rougher surface than the Al–4.5Cu–1.5Mg + 3WC composite.
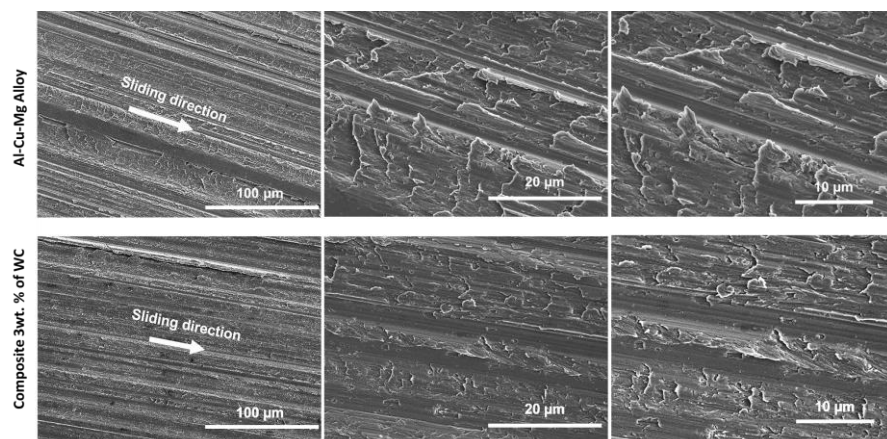

Figure 7. SEM secondary electron images from the worn surfaces in the Al–4.5Cu–1.5Mg alloy and the Al–4Cu –1.5Mg + 3WC composite. The samples correspond to the pin-on-disc test using 180 grit sizes of SiC abrasive sandpaper under 5 N of load and a sliding distance of 300 m.

Figure 8 shows SEM backscattered electron images and EDX elemental mapping from the worn surface of the Al–4.5Cu–1.5Mg alloy (Figure 8a) and the Al–4Cu–1.5Mg + 3WC composite (Figure 8b). From the worn surface of both samples, it was not easy to distinguish the nature of the particles present from their tonality, probably because of the roughness; for this reason, EDX elemental mappings were completed. The mappings for Figure 8a show only Cu-rich particles that correspond to the Al_2Cu phase. However, W-rich particles corresponding to the WC particles were observed in the composite (Figure 8b), consistent with the results shown in Figures 2 and 3. No preferential location of the Al_2Cu phase or the WC particles was observed, confirming the success of using the PM route to achieve a homogeneous dispersion of reinforcing particles. Mg and Al elements were detected across the matrix without the presence of Mg-rich phases, thus, suggesting Mg remained in a solid solution.
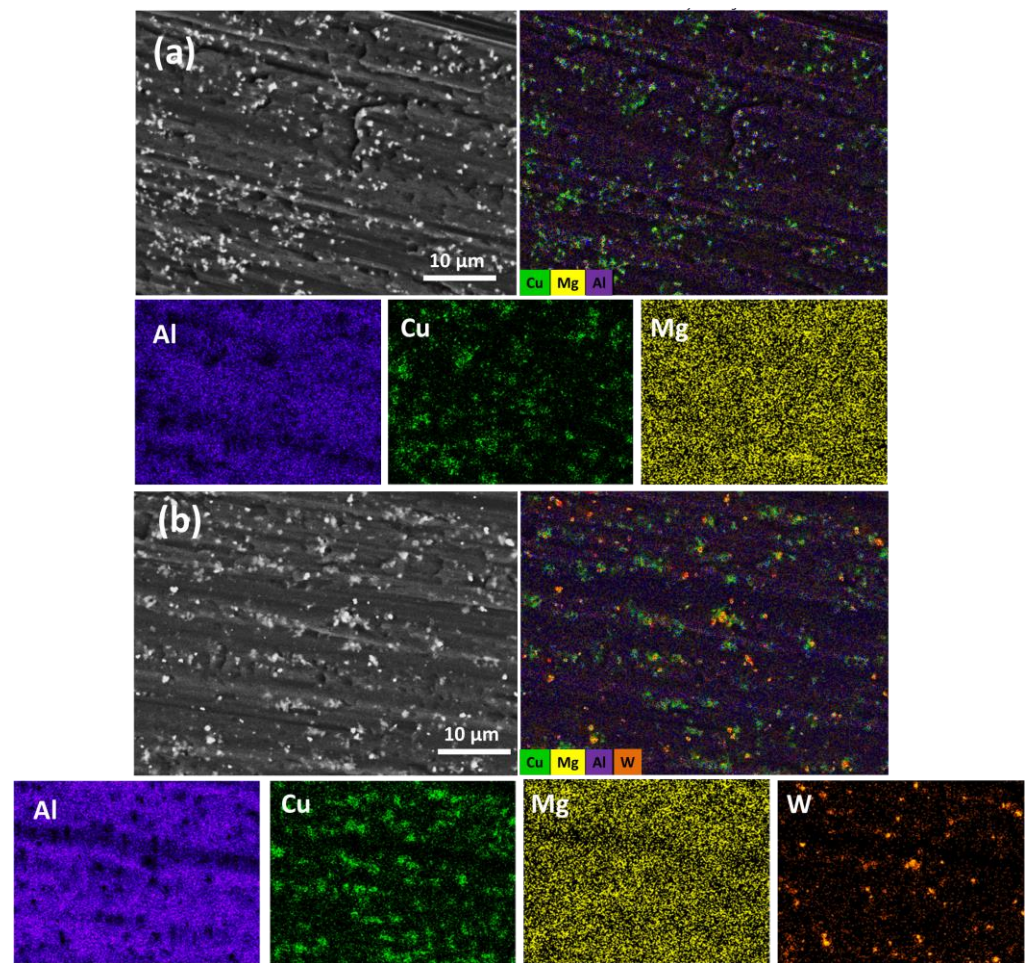
Figure 8. SEM backscattered electron images and EDX elemental mapping of the worn surface in the Al–4.5Cu–1.5Mg alloy (**a**) and the Al–4Cu–1.5Mg + 3WC composite (**b**). The mappings correspond to Al, Cu, Mg, and W elements, and the circle highlights delamination features.

4. Discussion

The wear rate is directly related to the applied load and the grit size of the abrasive sandpaper counterbody, which affects the groove depth, cutting capacity, and wear behavior [32,33]. For this study, in aggressive wear conditions (78 μm/180 number sandpaper), the composite reinforced with WC showed a lower wear rate, which could be attributed to the higher hardness of the composite due to the homogeneous distribution of reinforcing particles and the strong interfacial bonding. The strong WC particles/Al–Cu–Mg matrix interfacial bond provides a good load transfer capacity and restricts plastic deformation of the matrix, as reported by Rogriguez-Cabriales et al. [11]. Furthermore, Krishna et al. [15] pointed out that the wear resistance depends mainly on the hardness of the reinforcing particles, which is high for WC (1700 a 2400 HV) and comparable to SiC and TiC, ZrO, B_4C, and SnO_2 particles. Another important parameter for the wear behavior is the size of the reinforcing particles (coarse or fine) compared to the particles of the abrasive sandpaper (78, 52, and 22 μm). The ratio between the penetration depth and the reinforcing particle size is essential with coarse particles to determine the wear rate. However, when particles are fine (1000 mesh ~10 μm), the hardness of the composite controls the wear rate, leading to a higher friction coefficient and lower wear rate [28], as was the case studied in this research work. In addition, SiC abrasive sandpapers of number 400 (22 μm) led to a smaller decrease in wear rate in samples and similar wear behavior between the Al–Cu–Mg alloy and the composites. This behavior was attributed to the fact that for abrasives with large abrasive grit sizes sandpapers, the density of abrasive grains under the abraded surface

is lower, so the individual stress in each grain makes a greater contribution to the higher wear rate (increasing the quantity of material removed). On the contrary, the smaller-sized particles of abrasives sandpaper are only in elastic contact with a tested material and, thus, only support the applied load without contributing to the material removal [34]. Another important aspect is that the increased friction coefficient did not bring a rapid wear rate. This behavior was related to the enhanced deformation resistance also attributed to the high hardness, as was reported by Elhefnawey et al. [26]. It is known that the wear resistance and the hardness are related through the Archard equation (Equation (6)) [23].

$$Q = K\frac{W}{H} \tag{6}$$

where Q is the wear rate (mm^3/km), which is the volume of worn material per distance; W is the applied load; K is a constant called wear coefficient; and H is the hardness of the specimen in the Vickers scale (kg/mm^2). From the Archard equation, it is evident that the wear resistance of the materials is inversely proportional to the hardness, which agrees with the observations from Figures 3b and 5. In addition, the high hardness of the bulk composite occurred due to the strengthening mechanism caused by the hard particle dispersion, solid solution, and grain size reduction produced by mechanical milling [35].

The dominant wear mechanism in the studied systems was abrasive wear [23,36,37]. This mechanism was attributed to the superior hardness of the reinforcement that improved the sliding wear resistance of the matrix and generated a weathered surface that was smoother with the finest grooves and with lower plastic deformation than the Al–Cu–Mg alloy, which are typical features of abrasive wear [9,23,36,37]. Furthermore, due to a large number of load cycles, pits were initially formed, which promoted the formation of cracks on or below the surface, leading to delaminations [36,37]. According to the SEM results, the extension and size of the delamination were more significant for the sample without reinforcing particles. In this regard, the delamination theory by wear suggests that the surface and subsurface were deformed plastically due to the tangential force (i.e., shear force) acting upon the surface during sliding [38]. The addition of hard ceramic particles (WC) improved the wear resistance of the composites by having direct contact with the counterbody, preventing or decreasing the surface–subsurface deformation and, thus, protecting the softer Al matrix during abrasive sliding and strengthening the aluminum matrix. This behavior delayed the plastic deformation phenomena responsible for the degradation sequence [6,9], which was more evident when the conditions were more critical, i.e., when using sandpaper number 180 (78 μm) rather than sandpaper number 400 (22 μm).

5. Conclusions

The research presented in this paper has examined the effect of a 1, 2, and 3 WC wt. % addition on the wear behavior of Al–4Cu–1.5Mg/WC composites synthesized using powder metallurgy. From this work, the following conclusions have been drawn.

The aluminum Al–4Cu–1.5Mg alloy had a lower coefficient of friction (14%) than the alloys reinforced with 3 wt. % WC due to the lower values in hardness. In addition, when the abrasive grit size was larger (78 μm–180 number sandpaper), the Al–4Cu–1.5Mg alloy exhibited a higher wear rate than the WC-containing composites. However, the Al–4Cu–1.5Mg alloy behaved similarly to the composites when the abrasive grit size (22 μm/400 number sandpaper) of the counterbody was smaller due to the fact that for abrasives with large abrasive grit sizes sandpapers, the density of abrasive grains under the abraded surface was lower so that the individual stress in each grain was increasingly contributing to the higher wear rate. On the contrary, the smaller-sized particles of abrasives sandpaper were only in elastic contact with a tested material and, thus, only supported the applied load without contributing to material removal.

The characteristic grooves of abrasive wear and low signs of delamination indicated that the dominant wear mechanism was abrasive wear in Al–4Cu–1.5Mg/WC composites.

This mechanism was attributed to the superior hardness of the WC reinforcement, resulting in a 20% increase in the hardness of the composite containing 3 wt. % WC. Adding WC particles increased the resistance to sliding wear, resulting in a smoother worn surface with fewer deep grooves and less plastic deformation than the parent Al–4Cu–1.5Mg alloy.

Author Contributions: G.R.-C.: methodology, validation, formal analysis, investigation, writing—original draft, visualization. C.G.G.-R. and R.M.-S.: conceptualization, writing—original draft, supervision, review and editing, project administration. I.E.-G., M.A.R.-E.-R., J.M.M.-D., J.C.G.-T., H.M.M.-P., L.J.G.-H., S.G.-S. and K.A.G.-A.: methodology. All authors have read and agreed to the published version of the manuscript.

References

1. Zhang, J.; Song, B.; Wei, Q.; Bourell, D.; Shi, Y. A review of selective laser melting of aluminum alloys: Processing, microstructure, property and developing trends. *J. Mater. Sci. Technol.* **2019**, *35*, 270–284. [CrossRef]
2. Xiong, H.; Su, L.; Kong, C.; Yu, H. Development of High Performance of Al Alloys via Cryo-Forming: A Review. *Adv. Eng. Mater.* **2021**, *23*, 2001533. [CrossRef]
3. Barnwal, V.K.; Raghavan, R.; Tewari, A.; Narasimhan, K.; Mishra, S.K. Effect of microstructure and texture on forming behaviour of AA-6061 aluminium alloy sheet. *Mater. Sci. Eng. A* **2017**, *679*, 56–65. [CrossRef]
4. Fernández-López, P.; Alves, S.A.; López-Ortega, A.; San José-Lombera, J.T.; Bayon, R. High performance tribological coatings on a secondary cast Al–Si alloy generated by Plasma Electrolytic Oxidation. *Ceram. Int.* **2021**, *47*, 31238–31250. [CrossRef]
5. Kumar, H.P.; Xavior, M.A. Assessment of mechanical and tribological properties of Al 2024-SiC-graphene hybrid composites. *Procedia Eng.* **2017**, *174*, 992–999. [CrossRef]
6. Lekatou, A.; Karantzalis, A.E.; Evangelou, A.; Gousia, V.; Kaptay, G.; Gácsi, Z.; Gácsi, Z.; Baumli, P.; Simon, A. Aluminium reinforced by WC and TiC nanoparticles (ex-situ) and aluminide particles (in-situ): Microstructure, wear and corrosion behaviour. *Mater. Des.* **2015**, *65*, 1121–1135. [CrossRef]
7. Sathish, T.; Karthick, S. Wear behaviour analysis on aluminium alloy 7050 with reinforced SiC through taguchi approach. *J. Mater. Res. Technol.* **2020**, *9*, 3481–3487. [CrossRef]
8. Fernández, R.; Cabeza, S.; Mishurova, T.; Fernández-Castrillo, P.; González-Doncel, G.; Bruno, G. Residual stress and yield strength evolution with annealing treatments in an age-hardenable aluminum alloy matrix composite. *Mater. Sci. Eng. A* **2018**, *731*, 344–350. [CrossRef]
9. Mazahery, A.; Shabani, M.O. Influence of the hard coated B4C particulates on wear resistance of Al–Cu alloys. *Compos. Part B: Eng.* **2012**, *43*, 1302–1308. [CrossRef]
10. Soltani, S.; Azari Khosroshahi, R.; Taherzadeh Mousavian, R.; Jiang, Z.Y.; Fadavi Boostani, A.; Brabazon, D. Stir casting process for manufacture of Al–SiC composites. *Rare Met.* **2017**, *36*, 581–590. [CrossRef]
11. Rodríguez-Cabriales, G.; Lometo-Sánchez, A.M.; Guía-Tello, J.C.; Medrano-Prieto, H.M.; Gutiérrez-Castañeda, E.J.; Estrada-Guel, I.; Garay-Reyes, C.; Hernández-Rivera, J.; Cruz-Rivera, J.; Maldonado-Orozco, M.; et al. Synthesis and characterization of Al-Cu-Mg system reinforced with tungsten carbide through powder metallurgy. *Mater. Today Commun.* **2020**, *22*, 100758. [CrossRef]
12. Simon, A.; Lipusz, D.; Baumli, P.; Balint, P.; Kaptay, G.; Gergely, G.; Sfikas, A.; Lekatou, A.; Karantzalis, A.; Gacsi, Z. Microstructure and mechanical properties of Al-WC composites. *Arch. Metall. Mater.* **2015**, *60*, 1517–1521. [CrossRef]
13. Al-Mosawi, B.T.; Wexler, D.; Calka, A. Characterization and mechanical properties of α-Al$_2$O$_3$ particle reinforced aluminium matrix composites, synthesized via uniball magneto-milling and uniaxial hot pressing. *Adv. Powder Technol.* **2017**, *28*, 1054–1064. [CrossRef]
14. Pandiyan, A.; Kumar, G.A.; Ranganthan, S.; Madhu, S. Optimization of wear performance on aluminium die cast A360-M1 master alloy using response surface method. *Mater. Today Proc.* **2020**, *22*, 551–557. [CrossRef]
15. Krishna, U.B.; Vasudeva, B.; Auradi, V.; Nagaral, M. Effect of percentage variation on wear behaviour of tungsten carbide and cobalt reinforced Al7075 matrix composites synthesized by melt stirring method. *J. Bio-Tribo-Corros.* **2021**, *7*, 1–8. [CrossRef]

16. Pal, A.; Poria, S.; Sutradhar, G.; Sahoo, P. Tribological behavior of Al-WC nano-composites fabricated by ultrasonic cavitation assisted stir-cast method. *Mater. Res. Express* **2018**, *5*, 036521. [CrossRef]

17. Gowda, K.P.; Prakash, J.N.; Gowda, S.; Babu, B.S. Effect of particulate reinforcement on the mechanical properties of Al2024-WC MMCs. *J. Miner. Mater. Charact. Eng.* **2015**, *3*, 469–476. [CrossRef]

18. Mosbah, A.Y.; Wexler, D.; Calka, A. Abrasive wear of WC–FeAl composites. *Wear* **2005**, *258*, 1337–1341. [CrossRef]

19. Majzoobi, G.H.; Rahmani, K.; Atrian, A. Temperature effect on mechanical and tribological characterization of Mg–SiC nanocomposite fabricated by high rate compaction. *Mater. Res. Express* **2018**, *5*, 015046. [CrossRef]

20. Rahmani, K.; Majzoobi, G.H. The effect of particle size on microstructure, relative density and indentation load of Mg-B4C composites fabricated at different loading rates. *J. Compos. Mater.* **2020**, *54*, 2297–2311. [CrossRef]

21. Pérez-Bustamante, R.; Bueno-Escobedo, J.L.; Jiménez-Lobato, J.; Estrada-Guel, I.; Miki-Yoshida, M.; Licea-Jiménez, L.; Martínez-Sánchez, R. Wear behavior in Al2024–CNTs composites synthesized by mechanical alloying. *Wear* **2012**, *292*, 169–175. [CrossRef]

22. *ASTM G99-17*; Standard Test Method for Wear Testing with A Pin-On-Disk Apparatus. ASTM International: West Conshohocken, PA, USA, 2017.

23. Nemati, N.; Khosroshahi, R.; Emamy, M.; Zolriasatein, A. Investigation of microstructure, hardness and wear properties of Al–4.5 wt.% Cu–TiC nanocomposites produced by mechanical milling. *Mater. Des.* **2011**, *32*, 3718–3729. [CrossRef]

24. Prakash, N.A.; Gnanamoorthy, R.; Kamaraj, M. Friction and wear behavior of surface nanocrystallized aluminium alloy under dry sliding condition. *Mater. Sci. Eng. B* **2010**, *168*, 176–181. [CrossRef]

25. Huang, Y.; Fan, H.; Wang, D.; Sun, Y.; Liu, F.; Shen, J.; Sun, J.; Mi, J. The effect of cooling rate on the wear performance of a ZrCuAlAg bulk metallic glass. *Mater. Des.* **2014**, *58*, 284–289. [CrossRef]

26. Elhefnawey, M.; Shuai, G.L.; Li, Z.; Nemat-Alla, M.; Zhang, D.T.; Li, L. On dry sliding wear of ECAPed Al-Mg-Zn alloy: Wear rate and coefficient of friction relationship. *Alex. Eng. J.* **2021**, *60*, 927–939. [CrossRef]

27. Moheimani, S.K.; Keshtgar, A.; Khademzadeh, S.; Tayebi, M.; Rajaee, A.; Saboori, A. Tribological behaviour of AZ31 magnesium alloy reinforced by bimodal size B4C after precipitation hardening. *J. Magnes. Alloy.* **2021**, *10*, 3267–3280. [CrossRef]

28. Rahimian, M.; Parvin, N.; Ehsani, N. Investigation of particle size and amount of alumina on microstructure and mechanical properties of Al matrix composite made by powder metallurgy. *Mater. Sci. Eng. A* **2010**, *527*, 1031–1038. [CrossRef]

29. Abarghouie, S.M.; Reihani, S.S. Investigation of friction and wear behaviors of 2024 Al and 2024 Al/SiCp composite at elevated temperatures. *J. Alloys Compd.* **2010**, *501*, 326–332. [CrossRef]

30. Li, C.; Li, S.; Liu, C.; Zhang, Y.; Deng, P.; Guo, Y.; Wang, J.; Wang, Y. Effect of WC addition on microstructure and tribological properties of bimodal aluminum composite coatings fabricated by laser surface alloying. *Mater. Chem. Phys.* **2019**, *234*, 9–15. [CrossRef]

31. Weng, Z.; Wang, A.; Wu, X.; Wang, Y.; Yang, Z. Wear resistance of diode laser-clad Ni/WC composite coatings at different temperatures. *Surf. Coat. Technol.* **2016**, *304*, 283–292. [CrossRef]

32. Kaushik, N.; Sri Chaitanya, C.; Rao, R.N. Abrasive grit size effect on wear depth of stir cast hybrid Al–Mg–Si composites at high stress condition. *Proc. Inst. Mech. Eng. Part J J. Eng. Tribol.* **2018**, *232*, 672–684. [CrossRef]

33. Kök, M. Abrasive wear of Al2O3 particle reinforced 2024 aluminium alloy composites fabricated by vortex method. *Compos. Part A Appl. Sci. Manuf.* **2006**, *37*, 457–464. [CrossRef]

34. Kök, M.; Özdin, K. Wear resistance of aluminium alloy and its composites reinforced by Al2O3 particles. *J. Mater. Process. Technol.* **2007**, *183*, 301–309. [CrossRef]

35. Suryanarayana, C. Mechanical alloying and milling. *Prog. Mater. Sci.* **2001**, *46*, 1–184. [CrossRef]

36. Ergül, E.; Kurt, H.İ; Oduncuoğlu, M.; Can, Ç.İ.V.İ. Wear Properties of Al-Cu-Mg Composites Reinforced with MGO and MWCNT under Different Loads. *Int. J. Mater. Eng. Technol.* **2020**, *2*, 70–75.

37. Rao, R.N.; Devi, S.T. Wear regimes of Al-Cu-Mg matrix composites. *Composites* **2013**, *5*, 6. [CrossRef]

38. Hidalgo-Hernandez, R.G.; Plaza, N.; Suárez, O.M. A study on tribological characterization of Al-Cu-Mg-B composites subjected to mechanical wear. *Sci. Eng. Compos. Mater.* **2014**, *21*, 333–339. [CrossRef]